

Processes Associated with the Tropical Indian Ocean Subsurface Temperature Bias in a Coupled Model

J. S. CHOWDARY, ANANT PAREKH, G. SRINIVAS, AND C. GNANASEELAN

Indian Institute of Tropical Meteorology, Pune, India

T.S. FOUSIYA AND RASHMI KHANDEKAR

*Indian Institute of Tropical Meteorology, and Department of Atmospheric and Space Sciences,
Savitribai Phule Pune University, Pune, India*

M. K. ROXY

Indian Institute of Tropical Meteorology, Pune, India

(Manuscript received 10 December 2015, in final form 15 June 2016)

ABSTRACT

Subsurface temperature biases in coupled models can seriously impair their capability in generating skillful seasonal forecasts. The National Centers for Environmental Prediction (NCEP) Climate Forecast System, version 2 (CFSv2), coupled model, which is used for seasonal forecast in several countries including India, displays warm (cold) subsurface (surface) temperature bias in the tropical Indian Ocean (TIO), with deeper than observed mixed layer and thermocline. In the model, the maximum warm bias is reported between 150- and 200-m depth. Detailed analysis reveals that the enhanced vertical mixing by strong vertical shear of horizontal currents is primarily responsible for TIO subsurface warming. Weak upper-ocean stability corroborated by surface cold and subsurface warm bias further strengthens the subsurface warm bias in the model. Excess inflow of warm subsurface water from Indonesian Throughflow to the TIO region is partially contributing to the warm bias mainly over the southern TIO region. Over the north Indian Ocean, Ekman convergence and downwelling due to wind stress bias deepen the thermocline, which do favor subsurface warming. Further, upper-ocean meridional and zonal cells are deeper in CFSv2 compared to the Ocean Reanalysis System data manifesting the deeper mixing. This study outlines the need for accurate representation of vertical structure in horizontal currents and associated vertical gradients to simulate subsurface temperatures for skillful seasonal forecasts.

1. Introduction

Subsurface characteristics of oceans have recently become a topic of great concern to climate modeling groups because of its significantly large role in climate variability and climate change (Ruiz et al. 2005; Xiang et al. 2012). This is especially true for the tropical Indian Ocean (TIO; 20°S to 20°N, 40° to 100°E), where subsurface temperature change shows detectable difference from that of the surface, both in magnitude and spatial distribution (Hastenrath and Greischar 1989; Xie et al. 2002). The subsurface in the Arabian Sea and eastern

TIO are generally characterized by warm and deep thermocline. Meanwhile, the southwest TIO (thermocline dome region) subsurface temperatures are cooler than the rest of the TIO due to the shallow mean thermocline induced by Ekman pumping. Anomalous subsurface warming over the eastern equatorial Indian Ocean (IO) is reported prior to deficient Indian summer monsoon years (Krishnan et al. 2006). First, two dominant empirical orthogonal function (EOF) modes of the TIO subsurface temperature are closely associated with the Indian Ocean dipole (IOD; Rao et al. 2002) and El Niño (Sayantani and Gnanaseelan 2015). Subsurface ocean conditions in the western and eastern IO are important for predicting IOD events (e.g., Luo et al. 2007). Strong subsurface temperature variability associated with IOD, Asian monsoon, and the tropospheric biennial oscillation is established earlier (Loschnigg et al. 2003).

Corresponding author address: J. S. Chowdary, Indian Institute of Tropical Meteorology, Dr. Homi Bhabha Rd., Pashan, Pune 411008, India.
E-mail: jasti@tropmet.res.in

These studies highlight the crucial role of TIO subsurface temperatures in influencing the monsoon climate and variability. Therefore, it is essential to have a realistic representation of subsurface temperature in coupled models for a skillful prediction of tropical climate from seasonal (Krishnan et al. 2006) to decadal time scales (Dunstone and Smith 2010).

An important concern is the difficulty in depicting the surface and subsurface temperature variability especially in the TIO in coupled models (Gildor and Naik 2005). Biases that appear in the ocean subsurface temperature and salinity alter the ocean circulation, sea level, vertical mixing, and the coupling between ocean and atmosphere (Brown et al. 2013). A deeper (shallower) thermocline is an indication of warmer (cooler) subsurface (Neelin and Latif 1998). Thus, accurate representation of the thermocline depth and subsurface temperature is important in coupled general circulation models. In the present study, the characteristics of TIO subsurface temperature biases (100 to 500 m) are examined in the National Centers for Environmental Prediction (NCEP) Climate Forecast System, version 2 (CFSv2; Saha et al. 2014), coupled model free run. We further investigated the mechanisms responsible for the subsurface temperature bias in the model.

Under the National Monsoon Mission of India, CFSv2 is selected as an operational model for dynamical monsoon prediction over the Indian region (<http://www.tropmet.res.in/monsoon/index.php>), and this model has also been widely used for global-scale forecast (Saha et al. 2014). Identification of biases and their possible sources would provide the much needed guidance for further improvement of the model (Chowdary et al. 2014; Goswami et al. 2014). CFSv2 is known to suffer from strong cold sea surface temperature (SST) bias over the TIO (De et al. 2016; Chowdary et al. 2016a). The recently developed Earth System Model based on CFSv2 framework, despite having improved ocean physics, also displayed similar cold SST bias over the TIO with considerable improvements elsewhere (Swapna et al. 2015). Some studies pointed out that the mixed layer bias in CFSv2 needs to be rectified, as it significantly modulates the monsoon intraseasonal variability and associated rainfall (e.g., Roxy et al. 2013). Apart from this, the CFSv2 subsurface temperature response to El Niño–Southern Oscillation is stronger and deeper in the TIO than in the tropical Atlantic (Wang et al. 2013). Further, deep thermocline and warm subsurface temperature biases in the equatorial IO are reported in CFSv2 (Achuthavarier et al. 2012; Chowdary et al. 2016a). However, none of the previous studies examined the causes for the TIO subsurface warm bias in CFSv2. Understanding the mechanisms responsible for subsurface ocean temperature bias

would help to improve the thermodynamics and dynamics of the coupled model. In this study, emphasis is given to the annual-mean temperature bias and its vertical distribution over TIO. The rest of the paper is organized as follows: Section 2 provides model details and methodology. Model subsurface temperature biases are discussed in section 3. Processes associated with the subsurface biases are presented in section 4. Section 5 is summary and discussion.

2. Model and methodology

CFSv2 is a fully coupled ocean–atmosphere–land model with advanced physics and increased/finer resolution (Saha et al. 2014). The NCEP Global Forecast System (GFS) is the atmospheric component with horizontal resolution T126 (~100 km) and 64 sigma layers vertically. The oceanic component is the Modular Ocean Model, version 4 (MOM4P0; Griffies et al. 2004), from the Geophysical Fluid Dynamics Laboratory; zonal resolution is 0.5° , and the meridional resolution is 0.25° between 10°S to 10°N and gradually changes poleward through the tropics up to 0.5° . The model is integrated over a period of 100 yr, and the climatology of the last 60 yr is used for the present study. More details of CFSv2 integrations are provided by Roxy (2014). European Centre for Medium-Range Weather Forecasts (ECMWF) interim reanalysis (ERA-Interim; Dee et al. 2011) surface winds are used to explore wind biases in the coupled model. CFSv2 ocean component is evaluated against *World Ocean Atlas 2013 (WOA13)* temperature and salinity (Locarnini et al. 2013; Zweng et al. 2013) and ECMWF Ocean Reanalysis System 4 (ORAS4; Balmaseda et al. 2013) three-dimensional ocean currents. ORAS4 climatology is prepared based on the period 1979–2014. Nyadjro and McPhaden (2014) demonstrated that ORAS4 reproduces the horizontal current field in the TIO region reasonably well as compared to in situ observations. K-profile parameterization (KPP; Large et al. 1994) vertical mixing scheme is used in both CFSv2 and the model of ORAS4. The ocean mixed layer depth (MLD) is computed based on density variations determined from the corresponding temperature change of 0.8°C from the surface (Kara et al. 2003). The 20°C isotherm depth (D20) is utilized as a proxy for thermocline in the TIO. To understand the influence of stability, buoyancy, or Brunt–Väisälä frequency N^2 , energy required for mixing (ERM) and vertical turbulent eddy heat flux (VTHF) are computed. In addition to this, the vertical shear of horizontal currents is also computed to understand the mixing in CFSv2 and is compared to ORAS4. The equations used for understanding the physical mechanisms related to subsurface temperature bias are provided below:

$$\text{Brunt-Väisälä frequency is } N^2 = -\frac{g}{\rho} \frac{\partial \rho}{\partial z}; \quad (1)$$

$$\text{vertical shear is } \frac{dU}{dZ} = \sqrt{\left(\frac{\partial u}{\partial z}\right)^2 + \left(\frac{\partial v}{\partial z}\right)^2}; \quad (2)$$

$$\begin{aligned} \text{energy required for mixing is ERM} \\ = (1/8)(\rho_b - \rho_s)gh^2; \quad \text{and} \end{aligned} \quad (3)$$

$$\begin{aligned} \text{vertical turbulent eddy heat flux is } Q_z \\ = -\rho C_p K_h \left(\frac{\partial T}{\partial z} - \gamma\right). \end{aligned} \quad (4)$$

Horizontal and vertical advection includes the

$$\text{zonal advection term } u(\partial T/\partial x), \quad \text{and} \quad (5)$$

$$\text{meridional advection term } v(\partial T/\partial y). \quad (6)$$

Here, g is acceleration due to gravity (9.8 m s^{-2}), ρ is density of seawater (1029 kg m^{-3}), T is temperature ($^{\circ}\text{C}$), ρ_s is surface layer density (kg m^{-3}), ρ_b is bulk layer density (kg m^{-3}), h is MLD (m), C_p is specific heat of seawater ($4 \times 10^3 \text{ J kg}^{-1} \text{ }^{\circ}\text{C}^{-1}$), K_h is vertical eddy diffusivity ($\text{m}^2 \text{ s}^{-1}$) for ocean based on KPP, γ is nonlocal transport ($^{\circ}\text{C s}^{-1}$) term (Griffies 2012), u is zonal velocity (m s^{-1}), and v is meridional velocity (m s^{-1}). Vertical shear and other components are computed first at each grid point for each month and then the annual mean is computed and an area average performed to complete the analysis.

3. TIO subsurface temperature bias in CFSv2

The cold bias in TIO SST is common to almost all phase 5 of the Coupled Model Intercomparison Project (CMIP5) climate models (Li and Xie 2012, 2014; Wang et al. 2014; Sandeep and Ajayamohan 2014; Sayantani et al. 2016) and in CFSv2 (Fig. 1a). In addition to the surface cold bias, strong warm bias below the thermocline is apparent in CFSv2 (Figs. 1b–d). Temperature bias in CFSv2 is calculated with respect to *WOA13*. Subsurface temperature bias in CFSv2 is more than 3°C over the western equatorial IO, Arabian Sea, and southeast TIO regions. It confirms that CFSv2 suffers from a severe subsurface warm bias over the entire TIO. On the other hand, surface salinity bias is positive in the entire TIO region with the maximum being located over the Bay of Bengal (Fig. 1e). Excessive evaporation rather than insufficient precipitation in CFSv2 are mainly responsible for positive surface salinity bias over the TIO (Parekh et al. 2016; Chowdary et al. 2016b). Subsurface (~ 100 to 200 m) salinity bias is maximum over the Arabian Sea (Figs. 1e–h). Annual-mean spatial distribution of MLD reveals the existence of deeper MLD in CFSv2, as compared to

observations in the TIO except over the eastern and central equatorial IO (Fig. 2a). CFSv2 also displays strong positive bias in thermocline depth (D20) over the Arabian Sea and southern TIO (Fig. 2b). These deep MLD and D20 in the model indicate misrepresentation of vertical thermohaline structure and mixing in CFSv2.

The vertical structures of temperature, salinity, and density in the TIO are the defining features for many oceanic processes. The annual-mean vertical profiles of temperature, salinity, and density averaged over the TIO are shown in Figs. 3a–c, respectively, for CFSv2 and *WOA13*. Analysis of these vertical profiles reveals persistent cold bias of up to 1°C in the upper 80 m in CFSv2 (Fig. 3d) and warm subsurface bias exceeding 2°C around 175 m, which is consistent with the spatial temperature bias (Fig. 1). Overestimation of salinity averaged over TIO (Fig. 3b) is noted in the upper ocean and which is clearly reflected in the bias as well (Fig. 3e). Salinity bias is slightly higher around 175-m depth similar to temperature bias. Such large TIO subsurface temperatures and salinity biases in CFSv2 affect the vertical density structure (Fig. 3c). In fact, the model density indicates positive biases in the upper 100 m and negative biases below that, as compared to *WOA13* (Fig. 3f). Further regional analysis of vertical profiles of the biases over the Arabian Sea (6° – 23°N , 50° – 72°E), the Bay of Bengal (6° – 20°N , 80° – 95°E), eastern equatorial Indian Ocean (0° – 10°S , 90° – 100°E), and southwestern Indian Ocean thermocline dome region (5° – 10°S , 50° – 80°E) are in general consistent with the TIO mean bias nature (Figs. 3g–i), though their magnitudes are different for different basins (e.g., Chowdary et al. 2016b). This indicates that the nature of the vertical structure of bias is independent of the regional effect but could be due to discrepancy in the upper-ocean physics in the model. Hence, the unexplored factors responsible for subsurface biases are to be explored in detail.

4. Mechanisms associated with the subsurface bias

As the density bias of the upper ocean (subsurface) is more positive (negative) than observations in CFSv2, we have examined the Brunt–Väisälä frequency N^2 , which quantifies the stability of the stratified fluid (Gill 1982). Figure 4a shows N^2 profile of CFSv2 and *WOA13* in the TIO. The stability is relatively weaker in CFSv2 for the upper 150 m than the observed, which is apparent in the bias as well (Fig. 4e). On the other hand, stability is higher than *WOA13* below 200 m in CFSv2. Figure 4b shows the ERM for the upper 500 m. It is evident that the ERM is underestimated in CFSv2 by up to 30%, especially in 30- to 175-m depth (Fig. 4f). Figure 4c displays the vertical shear of the horizontal current in

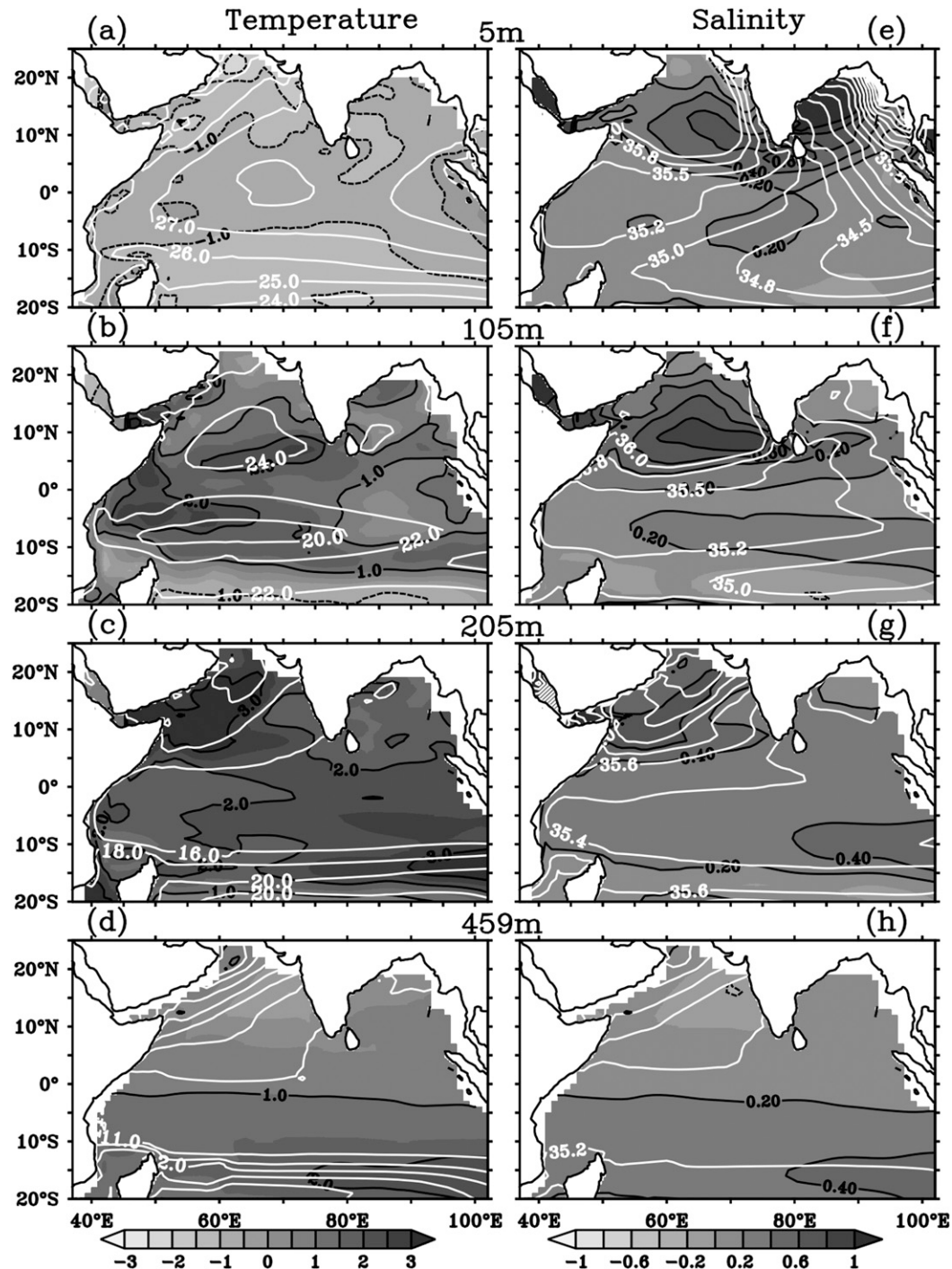


FIG. 1. CFSv2 annual-mean temperature (white contours; $^{\circ}\text{C}$) and bias (black contours and shaded; $^{\circ}\text{C}$) at depths (a) 5, (b) 105, (c) 205, and (d) 459 m over the TIO region. (e)–(h) As in (a)–(d), but for salinity (psu). Bias is calculated as the difference between CFSv2 and WOA13.

ORAS4 and CFSv2. Overestimation of shear in CFSv2 in the top 500 m is evident. It is important to note that the bias is about 200% (Fig. 4g) at around 150- to 250-m depth. Similar analysis is also carried out for the various regions

of TIO, since horizontal currents in the TIO are complex and have strong regional dependency. Thus, we have examined the vertical shear of horizontal currents in the Arabian Sea, Bay of Bengal, and equatorial Indian Ocean

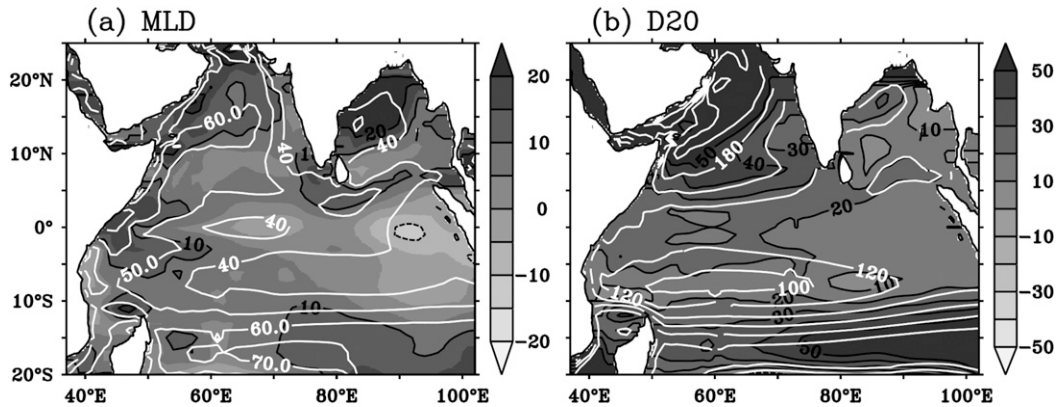


FIG. 2. (a) CFSv2 annual-mean mixed layer depth (white contour; m) and bias (black contours and shaded; m) and (b) mean thermocline (D20, 20°C isotherm) depth (white contour; m) and bias (black contours and shaded; m). Biases are calculated with respect to WOA13.

region (figure not shown) and found that bias in the vertical shear of horizontal currents in different basins also showed similar characteristics as in TIO, though the magnitude of the shear is different. Strong shear enhances the mixing of the upper ocean and weakens stability, leading to subsurface warming in the TIO. This excess mixing supports positive salinity bias in the upper few hundred meters. Further, vertical turbulent heat flux (Fig. 4d) has been computed using the KPP-based vertical eddy diffusivity K_h profile obtained from CFSv2. To estimate bias in CFSv2 VTHF, we have generated K_h from stand-alone ocean model MOM5 (considered as a reference profile), which is forced with observed winds. According to Griffies (2012), the nonlocal transport term γ contributes to VTHF along with local term $\partial T/\partial z$ [(4)] and hence is included in the computation. It is clearly evident from Figs. 4d and 4h that the CFSv2 has overestimated VTHF in the upper 80m. This is consistent with the surface cold bias and subsurface warm bias in the model. Thus, VTHF also may partly contribute to warm subsurface bias over the TIO.

To check whether the overestimation of shear is caused by atmospheric processes or oceanic processes, we analyzed vertical shear of horizontal currents in a stand-alone ocean model (MOM5, the ocean component of the coupled model, which is forced by observed atmospheric forcing) and the NCEP Global Ocean Data Assimilation System (GODAS). Though temperature and salinity bias is weaker than CFSv2 in stand-alone models, strong vertical shear bias is present (figure not shown). Strong vertical shear in the horizontal current is responsible for excessive mixing in the stand-alone ocean model. Further, Fousiya et al. (2015) also reported overestimation of vertical shear in ocean models as well as reanalysis products, which assimilate observed

salinity and temperature data. Hence, overestimation of vertical shear is due to the inherent ocean model mixing limitations. Altogether, strong vertical current shear is primarily responsible for the subsurface warm bias. The resultant subsurface warming and surface cooling due to heat flux bias further weaken the stratification and provide a positive feedback between weaker upper-ocean stratification and subsurface warming.

The above discussion supports the fact that strong vertical shear and weak stratification are contributing to warm subsurface temperature and positive salinity bias in the model. However, it is important to examine the contribution from zonal and meridional advection, respectively, from eastern [Indonesian Throughflow (ITF)] and southern boundaries of the TIO. It is well established that many coupled models have large uncertainty in representing ITF (e.g., Sen Gupta et al. 2016). Figure 5a shows the depth–latitude zonal current along the eastern boundary (averaged between 110° and 115°E) for CFSv2 and ORAS4. It is clearly evident that the model is able to capture the mean zonal current structure associated with the ITF at the eastern boundary. However, bias in the zonal current shows stronger westward flow in CFSv2 than in ORAS4 for the upper 225m between 10°S to 12°S (Fig. 5b). Since the subsurface ITF water is warmer than that of the Indian Ocean (e.g., Zhou et al. 2008; Valsala and Maksyutov 2010), anomalous westward flow may have some contribution to subsurface warm temperature bias in TIO around 10°S (Figs. 1b–d). Weaker meridional current bias at the southern boundary is also seen in the model (Figs. 5c,d), suggesting that the excess warm water that entered from the throughflow is not completely taken out of TIO through the southern boundary. Thus, apart from the

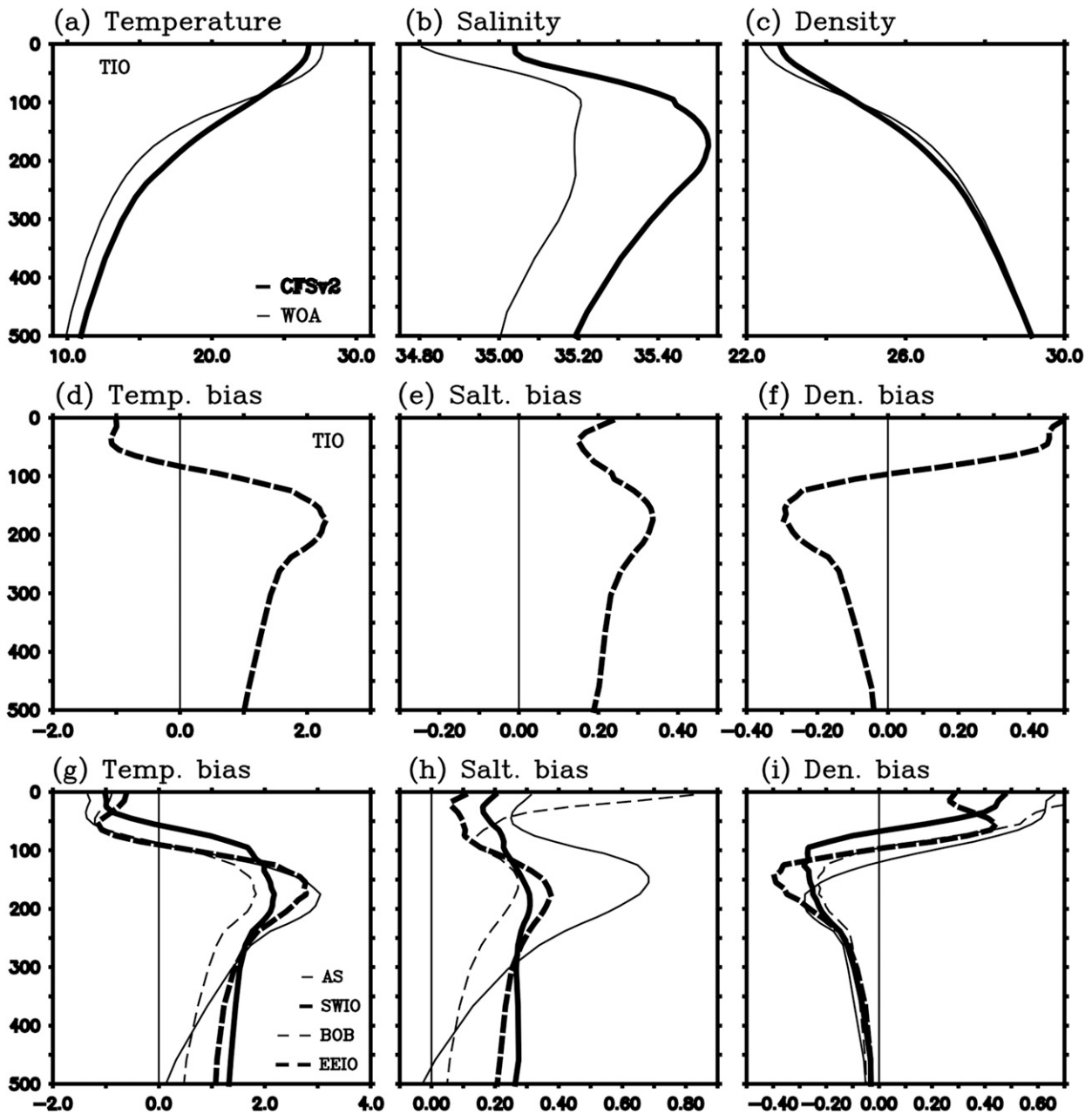


FIG. 3. Vertical profiles in upper 500 m [annual-mean area averaged in the TIO region (20°S–20°N, 40°–100°E)] for CFSv2 and WOA13. (a) Temperature (°C), (b) salinity (psu), and (c) density (kg m⁻³). (d)–(f) As in (a)–(c), but for bias. (g)–(i) As in (d)–(f), but for different regions of TIO [Bay of Bengal (BOB), Arabian Sea (AS), southwest Indian Ocean thermocline dome region (SWIO), and east equatorial Indian Ocean (EEIO)].

vertical mixing and weak stability, excess warm water advection from ITF also plays a partial role in the subsurface warm bias over the southern TIO. Contribution of advection through the eastern (at 100°E) and southern (20°S) boundaries to TIO temperature is illustrated in Figs. 5e and 5f. Contribution of zonal advection at the eastern boundary is up to 0.7°C s⁻¹ (maximum at 150 m) in

CFSv2 and 0.4°C s⁻¹ (maximum at 50 m) in ORAS4. However, actual TIO subsurface temperature bias is about 3 times that of ITF contribution. Meridional advection through the southern boundary is consistent with ORAS4. Therefore, the subsurface warm bias is mainly caused by excess vertical shear of horizontal currents' induced downward transfer of heat.

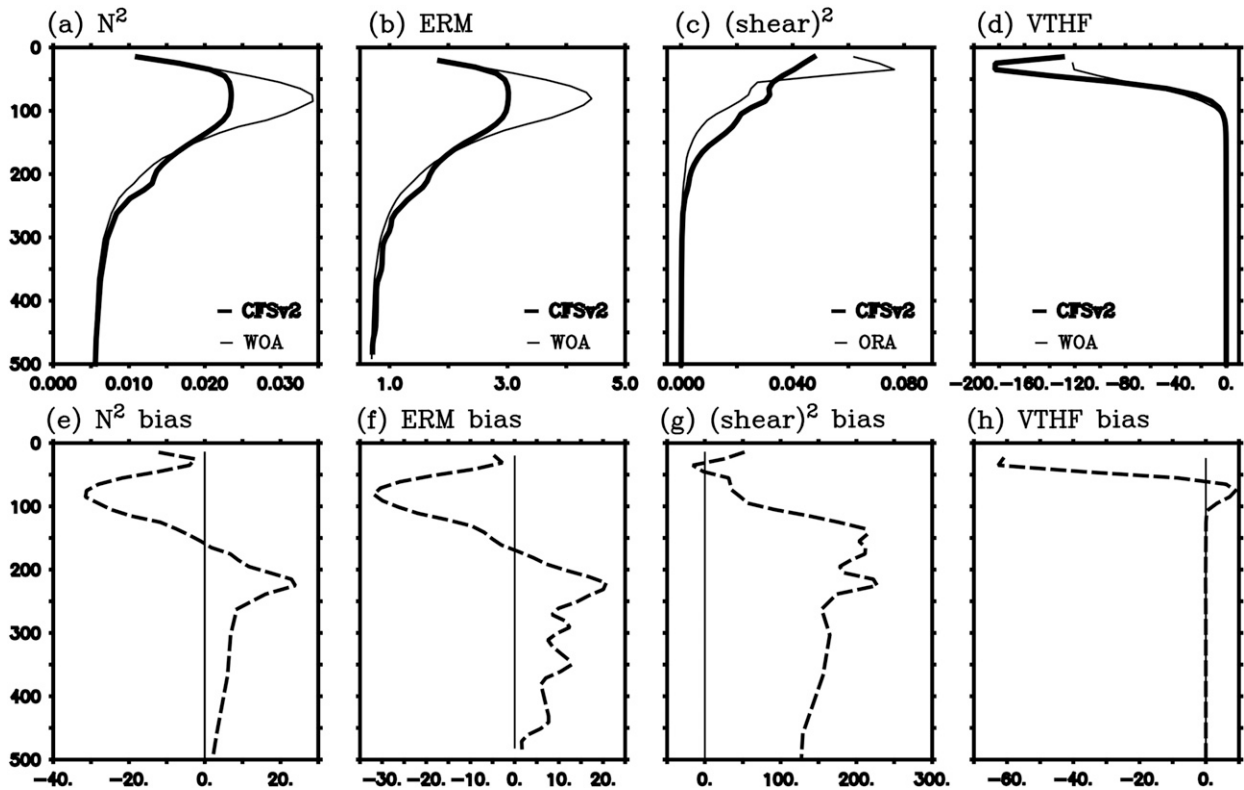


FIG. 4. Vertical profiles of (annual-mean area averaged in the TIO region) (a) Brunt-Väisälä frequency (N^2 ; 10^{-2} s^{-2}), (b) ERM (J m^{-2}), (c) square of the vertical shear of horizontal currents (10^{-4} s^{-2}), and (d) vertical turbulent heat flux (W m^{-2}). (e)-(h) As in (a)-(d), but for bias. Biases in N^2 profiles and ERM of CFSv2 are calculated with respect to WOA13. In the case of vertical shear, CFSv2 bias is calculated with respect to ORAS4. Vertical turbulent heat flux bias is with respect to WOA13/MOM5. Note that biases are normalized with respect to observations and are presented in percentage except for vertical turbulent heat flux.

The wind-induced changes in thermocline depth can alter subsurface temperatures (Xiang et al. 2012). Annual-mean surface wind speed from CFSv2 and ERA-Interim are provided in Figs. 6a and 6b, and it is found that the model is able to reproduce the spatial patterns of winds reasonably well. Figure 6c illustrates wind speed and wind vector bias over the TIO region. Note that model wind bias is calculated as the difference between CFSv2 and ERA-Interim. Positive wind speed bias is seen over most of the TIO. Thus, the strength of wind stirring is marginally higher and may affect the vertical mixing in the TIO, which in turn could influence the subsurface temperature bias. CFSv2 annual-mean wind bias exhibits strong easterlies over the western equatorial IO and anticyclonic circulation over the Arabian Sea and Bay of Bengal (Fig. 6c). This equatorial easterly wind bias could be due to improper representation of boreal summer monsoon circulation (e.g., Li et al. 2015a,b). Further, Ekman pumping shows negative bias in most of the north IO, suggesting that Ekman convergence is strong in CFSv2 compared to observations (Fig. 6d). Anomalous convergence deepens the thermocline due to downwelling and favors subsurface

warming. Surface wind bias over the central-southern TIO is southerly and the Ekman pumping bias is weak (Figs. 6c,d). Vertical velocity averaged from 100 to 150 m further supports this (Figs. 6e,f). However, much stronger upward velocity (positive) is noted over the equatorial region in CFSv2 as compared to ORAS4, which is consistent with wind bias. CFSv2 displays upward velocity somewhat similar to that of ORAS4 over the southwest TIO region (Figs. 6e,f). Overall, CFSv2 displays dominant upward velocities at the equator and downward velocities in the northern and southern TIO.

The extent of penetration of anomalous vertical velocities in CFSv2 is important for the subsurface temperature bias point of view. The depth-longitude plot of vertical velocities averaged between 20°S to 20°N for CFSv2 and ORAS4 are presented in Figs. 7a and 7b, respectively. The vertical velocity is much deeper and stronger in CFSv2 compared to ORAS4, especially west of 60°E. This suggests that CFSv2 has stronger mixing that extends to a deeper level than in ORAS4, which favors subsurface warming over the TIO. Similarly, the depth-latitude plot also shows that

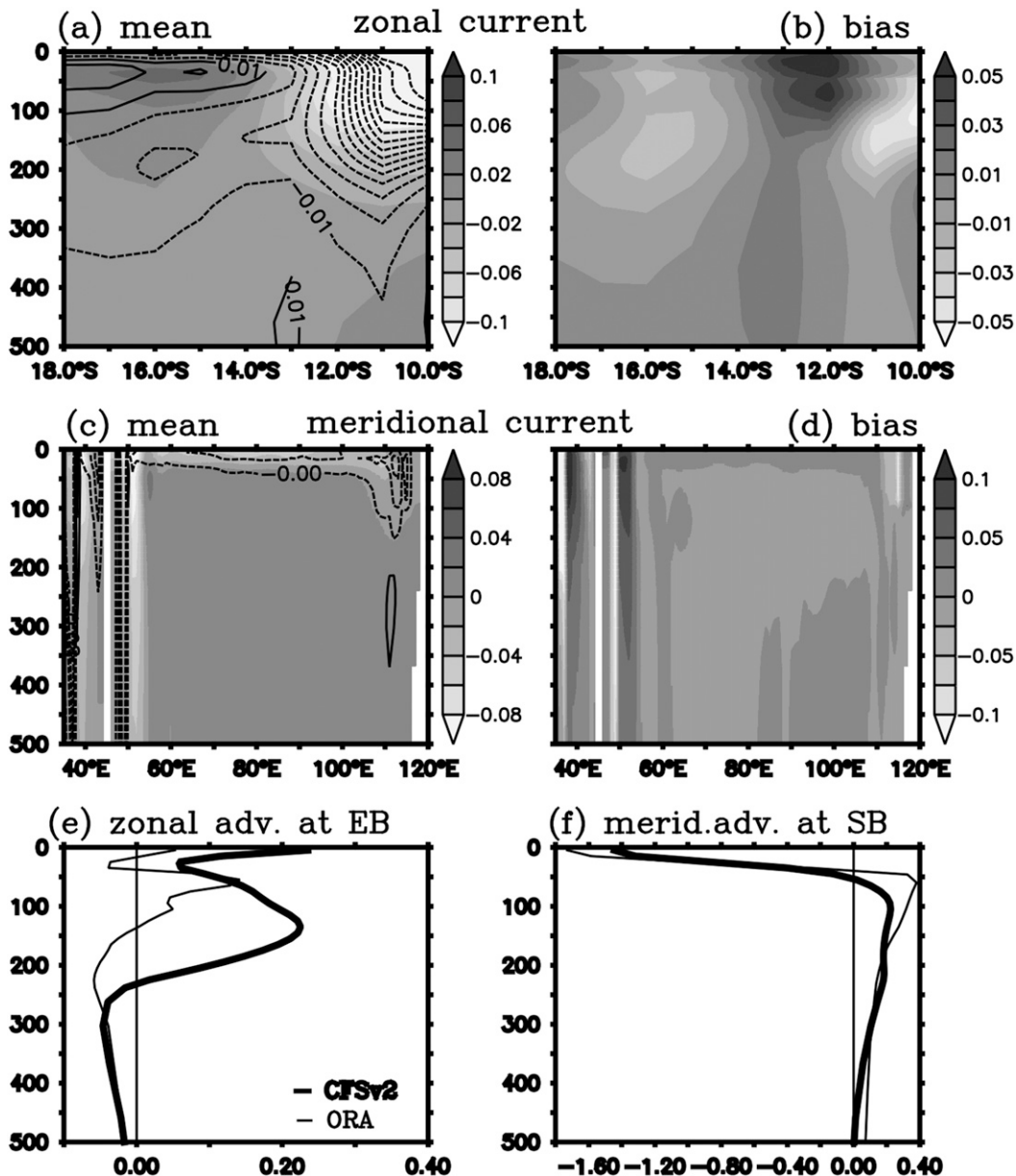


FIG. 5. Depth–latitude plot of mean zonal current averaged between 110° to 115°E for (a) ORAS4 (shaded; m s^{-1}) and CFSv2 (contours; m s^{-1}) and (b) bias (difference between CFSv2 and ORAS4). (c),(d) As in (a) and (b), but for depth–longitude plot for mean meridional current averaged between 20°S to 25°S . Contribution to temperature (vertical profiles) from (e) mean zonal advection at eastern boundary (100°E) averaged from 5° to 20°S ($10^{-7}^{\circ}\text{C s}^{-1}$) and (f) mean meridional advection ($10^{-7}^{\circ}\text{C s}^{-1}$) at southern boundary (20°S) averaged from 55° to 100°E for CFSv2 and ORAS4.

the upper-ocean meridional cell is deeper in CFSv2 compared to ORAS4 (Figs. 7c,d). This further supports the role of vertical advection in affecting the subsurface temperatures in the model.

In the case of SST, studies show that the cold bias over the TIO is usually associated with bias in MLD and heat flux (e.g., Wajswicz 2007). Figure 8a shows

the contribution of heat flux to mixed layer temperature/SST in CFSv2. As compared to the observations, contribution of heat flux to mixed layer temperature in the model is less over most of the TIO (Figs. 8a,b). As the MLD in CFSv2 is deeper than in observations, the model MLD is replaced by observed MLD, while estimating the contribution of MLD/mixing on mixed

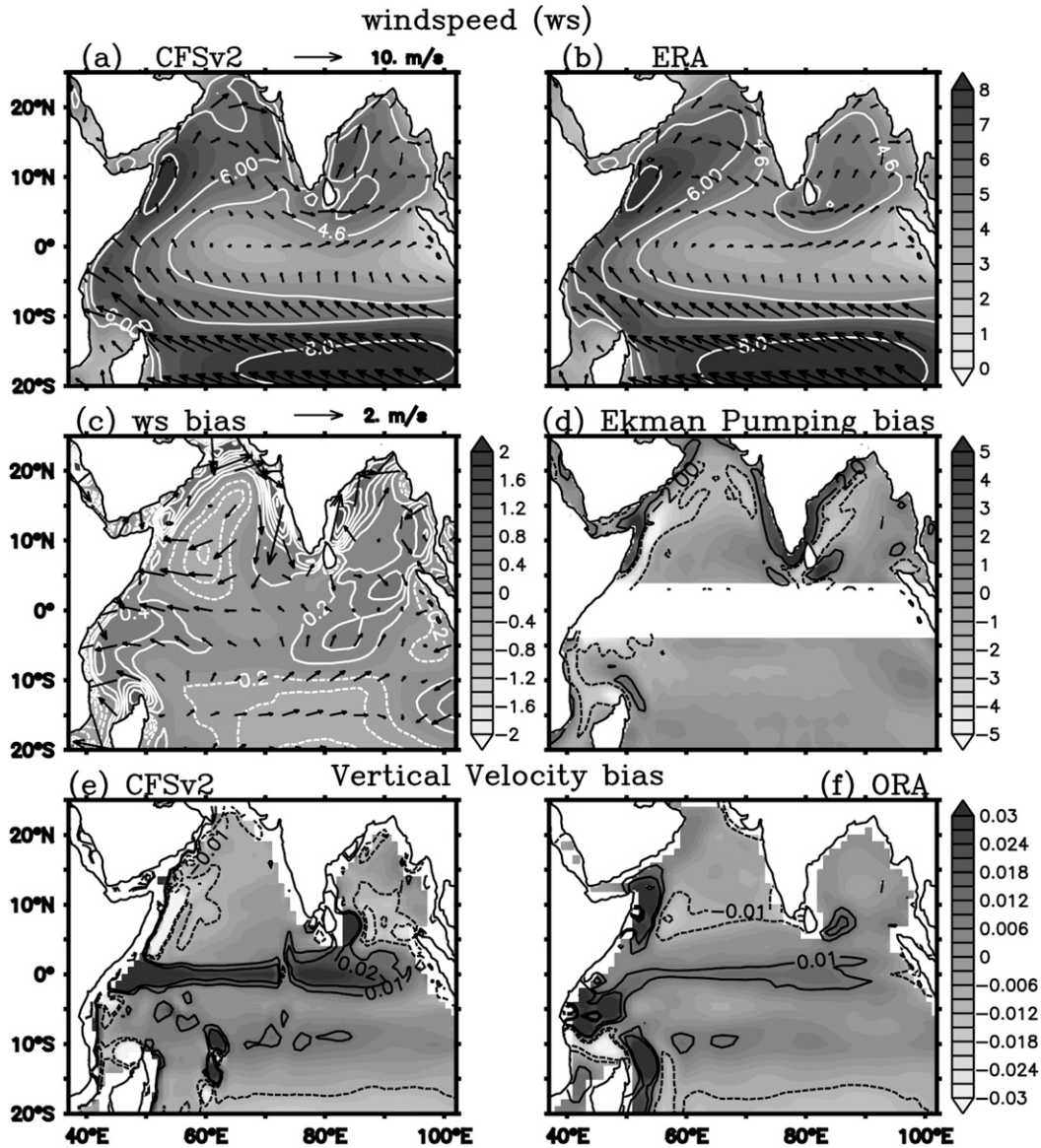


FIG. 6. Annual-mean surface wind speed (contour and shaded; $m s^{-1}$) and wind vectors ($m s^{-1}$) for (a) CFSv2 and (b) ERA, (c) bias of wind speed (contour and shaded; $m s^{-1}$) and wind vectors and (d) Ekman pumping velocity bias (contours and shaded; $10^{-6} m s^{-1}$), and (e) CFSv2 vertical velocity (contour and shaded; $10^{-4} m s^{-1}$) averaged between 100 and 150 m. (f) As in (e), but for ORAS4.

layer temperature, and is shown in Fig. 8c. Heat flux-only contribution to mixed layer temperature shows (Fig. 8d) negative contribution in CFSv2 over most of the southern TIO and west coast of India, and in the rest of the regions, contribution is positive. Figure 8e suggests that mixing also plays an important role in cooling upper-ocean temperature in CFSv2 over the TIO, except over the eastern equatorial IO and southeast TIO. The combined effect of heat flux and mixing on mixed layer temperature is displayed in Fig. 8f, which is high (negative) over most of TIO. This analysis suggests that

deep MLD in CFSv2 contributes to about 35% to 40% of the actual mixed layer temperature/SST cold bias in most of the TIO in CFSv2. TIO basinwide cold SST bias in CFSv2 is also associated with excess evaporation due to dry troposphere and underestimation of cloud amount (Hazra et al. 2015; Pokhrel et al. 2016; Chowdary et al. 2016a). In many climate models, tropical-wide cold SST biases are mainly due to uncertainties in cloud amount (Lin 2007; Li and Xie 2012). On the other hand, warm subsurface temperature is attributed to excessive upper-ocean mixing induced by

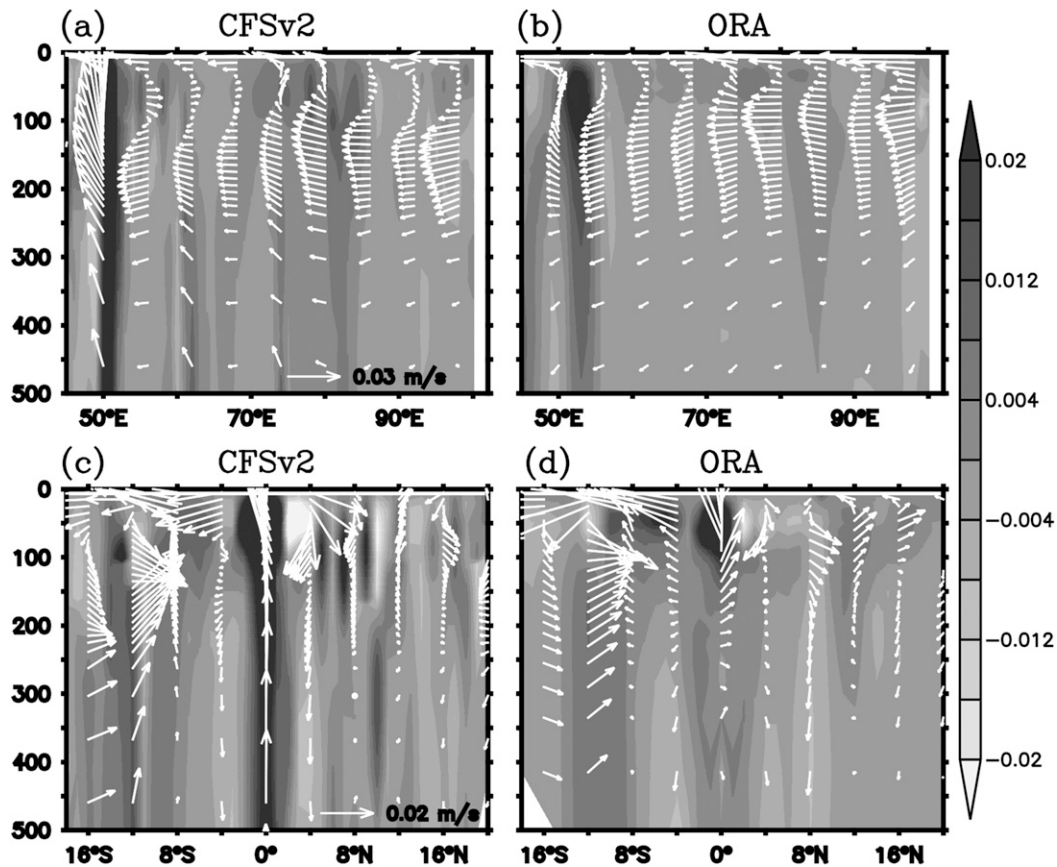


FIG. 7. (a) Depth–longitude plot of CFSv2 vertical and horizontal current (vector; m s^{-1}) and vertical current (shaded; 10^{-4} m s^{-1}) averaged over 20°S to 20°N . (b) As in (a), but for ORAS4. (c) Depth–latitude plot of CFSv2 vertical and horizontal current (vector; m s^{-1}) and vertical current (shaded; 10^{-4} m s^{-1}) averaged over 40° to 100°E . (d) As in (c), but for ORAS4.

vertical shear in the horizontal current and weaker stratification and to some extent from ITF warm water advection and poor representation of winds in the model.

5. Summary and discussion

Subsurface temperature may provide a source of memory for predicting coupled ocean–atmosphere modes (Jiang et al. 2013; Luo et al. 2007), which has considerable impact on monsoon and the tropical climate variability. Thus, understanding the subsurface temperature biases and associated mechanisms in a coupled model is important. The present study addresses the mechanisms that are responsible for the anomalous TIO warm bias in the subsurface in CFSv2, a coupled model widely used for monsoon forecast.

Cold bias in the upper 80 m and warm bias below in the TIO region are typical features of CFSv2 over the

TIO region. Subsurface temperature bias is maximum around 175-m depth with values exceeding 2°C . Apart from this, the vertical profiles of salinity and density display anomalous surface and subsurface bias in CFSv2. Analysis reveals that strong vertical shear in horizontal currents in the model paves the way for a deeper penetration of the warm waters, resulting in the subsurface warm bias. Corroborated by anomalously strong vertical shear with surface cold and subsurface warm biases, the underestimated upper-ocean stratification in CFSv2 is further feedback to subsurface warm bias. These processes favor enhanced mixing of warm surface water with subsurface water. Apart from this, excess Indonesian Throughflow warm water partly contributes to the southern TIO subsurface temperature bias. The equatorial current bias in CFSv2 is mainly due to the unrealistic representation of winds over the TIO, which is in phase with subsurface warm bias. Surface winds also display strong anticyclonic circulation bias over the Arabian Sea and

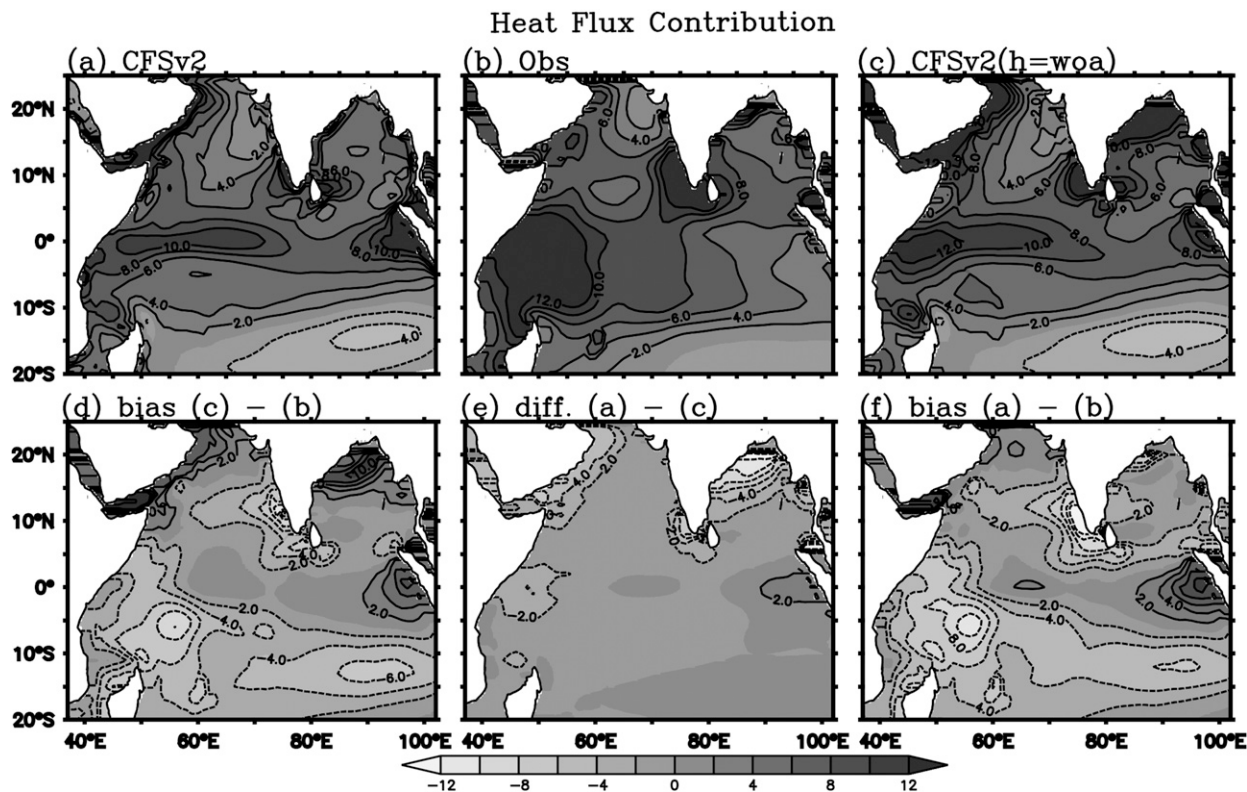


FIG. 8. (a) Contribution of net heat flux to mixed layer temperature (CFSv2 $Q_{net}/\rho c_p h$; where mixed layer depth h is from CFSv2). (b) As in (a), but Q_{net} from Tropflux and h from WOA13. (c) As in (a), but Q_{net} is from CFSv2 and h is from WOA13. (d) Heat flux (Q_{net})–only contribution to SST bias, which is (c) minus (b); (e) contribution of mixed layer depth, which is (a) minus (c); and (f) contribution of heat flux and h ($Q_{net}/\rho c_p h$), which is (a) minus (b). Units are $^{\circ}\text{C}$.

Bay of Bengal. In response to wind bias, anomalous Ekman convergence and associated downwelling helped to sustain subsurface warming. Upper-ocean zonal and meridional cells are found to be deeper in CFSv2 compared to ORAS4. These further support the importance of vertical processes in affecting the subsurface temperatures in the model. Therefore, in order to improve the vertical thermal structure of TIO in CFSv2, it is essential to reduce the biases in vertical mixing processes.

Acknowledgments. We thank the director of ESSO-IITM and MoES for support. This work was funded by ESSO-IITM. The CFSv2 free run used in the study is available at IITM. (We have obtained ORAS4 data from <http://www.ecmwf.int/en/research/climate-reanalysis/ocean-reanalysis>, ERA-Interim from <http://www.ecmwf.int/en/research/climate-reanalysis/era-interim>, and WOA13 from <http://www.nodc.noaa.gov/OC5/woa13/>.) We sincerely thank the anonymous reviewers for their valuable comments that helped us to improve the manuscript. We thank Ms. Ananya Karmakar and Dr. Vinu Valsala for helpful discussions and providing data. Figures were prepared in Ferret.

REFERENCES

Achuthavarier, D., V. Krishnamurthy, B. P. Kirtman, and B. Huang, 2012: Role of Indian Ocean in the ENSO–Indian summer monsoon teleconnection in the NCEP climate forecast system. *J. Climate*, **25**, 2490–2508, doi:10.1175/JCLI-D-11-00111.1.

Balmaseda, M. A., K. Mogensen, and A. T. Weaver, 2013: Evaluation of the ECMWF ocean reanalysis system ORAS4. *Quart. J. Roy. Meteor. Soc.*, **139**, 1132–1161, doi:10.1002/qj.2063.

Brown, J. N., and Coauthors, 2013: Implications of CMIP3 model biases and uncertainties for climate projections in the western tropical Pacific. *Climatic Change*, **119**, 147–161, doi:10.1007/s10584-012-0603-5.

Chowdary, J. S., H. S. Chaudhari, C. Gnanaseelan, A. Parekh, A. S. Rao, P. Sreenivas, S. Pokhrel, and P. Singh, 2014: Summer monsoon circulation and precipitation over the tropical Indian Ocean during ENSO in the NCEP climate forecast system. *Climate Dyn.*, **42**, 1925–1947, doi:10.1007/s00382-013-1826-5.

—, A. Parekh, S. Ojha, C. Gnanaseelan, and R. Kakatkar, 2016a: Impact of upper ocean processes and air–sea fluxes on seasonal SST biases over the tropical Indian Ocean in the NCEP Climate Forecasting System. *Int. J. Climatol.*, **36**, 188–207, doi:10.1002/joc.4336.

—, G. Srinivas, T. S. Fousiya, A. Parekh, C. Gnanaseelan, H. Seo, and J. A. MacKinnon, 2016b: Representation of Bay of Bengal upper-ocean salinity in general circulation models. *Oceanography*, **29**, 38–49, doi:10.5670/oceanog.2016.37.

- De, S., A. Hazra, and H. S. Chaudhari, 2016: Does the modification in “critical relative humidity” of NCEP CFSv2 dictate Indian mean summer monsoon forecast? Evaluation through thermodynamical and dynamical aspects. *Climate Dyn.*, **46**, 1197–1222, doi:10.1007/s00382-015-2640-z.
- Dee, D. P., and Coauthors, 2011: The ERA-Interim reanalysis: Configuration and performance of the data assimilation system. *Quart. J. Roy. Meteor. Soc.*, **137**, 553–597, doi:10.1002/qj.828.
- Dunstone, N. J., and D. M. Smith, 2010: Impact of atmosphere and sub-surface ocean data on decadal climate prediction. *Geophys. Res. Lett.*, **37**, L02709, doi:10.1029/2009GL041609.
- Fousiya, T. S., A. Parekh, and C. Gnanaseelan, 2015: Interannual variability of upper ocean stratification in Bay of Bengal: Observational and modeling aspects. *Theor. Appl. Climatol.*, doi:10.1007/s00704-015-1574-z, in press.
- Gildor, H., and N. H. Naik, 2005: Evaluating the effect of interannual variations of surface chlorophyll on upper ocean temperature. *J. Geophys. Res.*, **110**, C07012, doi:10.1029/2004JC002779.
- Gill, A. E., 1982: *Atmosphere–Ocean Dynamics*. Academic Press, 662 pp.
- Goswami, B. B., M. S. Deshpande, P. Mukhopadhyay, S. K. Saha, A. S. Rao, R. Murthugudde, and B. N. Goswami, 2014: Simulation of monsoon intraseasonal variability in NCEP CFSv2 and its role on systematic bias. *Climate Dyn.*, **43**, 2725–2745, doi:10.1007/s00382-014-2089-5.
- Griffies, S., 2012: Elements of the Modular Ocean Model (MOM). NOAA GFDL Ocean Group Tech. Rep. 7, 618 pp. [Available online at http://www.mom-ocean.org/web/docs/project/MOM5_elements.pdf.]
- , M. J. Harrison, R. C. Pacanowski, and R. A. Anthony, 2004: A technical guide to MOM4. GFDL Ocean Group Tech. Rep. 5, 342 pp. [Available online at https://www.gfdl.noaa.gov/bibliography/related_files/smg0301.pdf.]
- Hastenrath, S., and L. L. Greischar, 1989: Climatic Atlas of the Indian Ocean: *Upper Ocean Structure*. University of Wisconsin Press, 274 pp.
- Hazra, A., H. S. Chaudhari, S. A. Rao, B. N. Goswami, A. Dhakate, S. Pokhrel, and S. K. Saha, 2015: Impact of revised cloud microphysical scheme in CFSv2 on the simulation of the Indian summer monsoon. *Int. J. Climatol.*, **35**, 4738–4755, doi:10.1002/joc.4320.
- Jiang, X. W., S. Yang, J. P. Li, Y. Q. Li, H. R. Hu, and Y. Lian, 2013: Variability of the Indian Ocean SST and its possible impacts on summer western North Pacific anticyclone in the NCEP Climate Forecast System. *Climate Dyn.*, **41**, 2199–2212, doi:10.1007/s00382-013-1934-2.
- Kara, A. B., P. A. Rochford, and H. E. Hurlburt, 2003: Mixed layer depth variability over the global ocean. *J. Geophys. Res.*, **108**, 3079, doi:10.1029/2000JC000736.
- Krishnan, R., K. V. Ramesh, B. K. Samala, G. Meyers, J. M. Slingo, and M. J. Fennessy, 2006: Indian Ocean-monsoon coupled interactions and impending monsoon droughts. *Geophys. Res. Lett.*, **33**, L08711, doi:10.1029/2006GL025811.
- Large, W. G., J. C. McWilliams, and S. C. Doney, 1994: Oceanic vertical mixing: A review and a model with a nonlocal boundary layer parameterization. *Rev. Geophys.*, **32**, 363–403, doi:10.1029/94RG01872.
- Li, G., and S.-P. Xie, 2012: Origins of tropical-wide SST biases in CMIP multi-model ensembles. *Geophys. Res. Lett.*, **39**, L22703, doi:10.1029/2012GL053777.
- , and —, 2014: Tropical biases in CMIP5 multimodel ensemble: The excessive equatorial Pacific cold tongue and double ITCZ problems. *J. Climate*, **27**, 1765–1780, doi:10.1175/JCLI-D-13-00337.1.
- , —, and Y. Du, 2015a: Monsoon-induced biases of climate models over the tropical Indian Ocean. *J. Climate*, **28**, 3058–3072, doi:10.1175/JCLI-D-14-00740.1.
- , —, and —, 2015b: Climate model errors over the south Indian Ocean thermocline dome and their effect on the basin mode of interannual variability. *J. Climate*, **28**, 3093–3098, doi:10.1175/JCLI-D-14-00810.1.
- Lin, J.-L., 2007: The double-ITCZ problem in IPCC AR4 coupled GCMs: Ocean–atmosphere feedback analysis. *J. Climate*, **20**, 4497–4525, doi:10.1175/JCLI4272.1.
- Locarnini, R. A., and Coauthors, 2013: *Temperature*. Vol. 1, *World Ocean Atlas 2013*, NOAA Atlas NESDIS 73, 40 pp.
- Loschnigg, J., G. A. Meehl, P. J. Webster, J. M. Arblaster, and G. P. Compo, 2003: The Asian monsoon, the tropospheric biennial oscillation, and the Indian Ocean zonal mode in the NCAR CSM. *J. Climate*, **16**, 1617–1642, doi:10.1175/1520-0442(2003)016<1617:TAMTTB>2.0.CO;2.
- Luo, J.-J., S. Masson, S. K. Behera, and T. Yamagata, 2007: Experimental forecasts of the Indian Ocean dipole using a coupled OAGCM. *J. Climate*, **20**, 2178–2190, doi:10.1175/JCLI4132.1.
- Neelin, J. D., and M. Latif, 1998: El Niño dynamics. *Phys. Today*, **51**, 32–36, doi:10.1063/1.882496.
- Nyadjro, E., and M. J. McPhaden, 2014: Variability of zonal currents in the eastern equatorial Indian Ocean on seasonal to interannual time scales. *J. Geophys. Res. Oceans*, **119**, 7969–7986, doi:10.1002/2014JC010380.
- Parekh, A., J. S. Chowdary, O. Sayantani, T. S. Fousiya, and C. Gnanaseelan, 2016: Tropical Indian Ocean surface salinity bias in Climate Forecasting System coupled models and the role of upper ocean processes. *Climate Dyn.*, **46**, 2403–2422, doi:10.1007/s00382-015-2709-8.
- Pokhrel, S., and Coauthors, 2016: Seasonal prediction of Indian summer monsoon rainfall in NCEP CFSv2: forecast and predictability error. *Climate Dyn.*, **46**, 2305–2326, doi:10.1007/s00382-015-2703-1.
- Rao, S. A., S. K. Behera, Y. Masumoto, and T. Yamagata, 2002: Interannual subsurface variability in the tropical Indian Ocean with a special emphasis on the Indian Ocean dipole. *Deep-Sea Res. II*, **49**, 1549–1572, doi:10.1016/S0967-0645(01)00158-8.
- Roxy, M., 2014: Sensitivity of precipitation to sea surface temperature over the tropical summer monsoon region and its quantification. *Climate Dyn.*, **43**, 1159–1169, doi:10.1007/s00382-013-1881-y.
- , Y. Tanimoto, B. Preethi, P. Terray, and R. Krishnan, 2013: Intraseasonal SST-precipitation relationship and its spatial variability over the tropical summer monsoon region. *Climate Dyn.*, **41**, 45–61, doi:10.1007/s00382-012-1547-1.
- Ruiz, J. E., I. Cordery, and A. Sharma, 2005: Integrating ocean subsurface temperatures in statistical ENSO forecasts. *J. Climate*, **18**, 3571–3586, doi:10.1175/JCLI3477.1.
- Saha, S., and Coauthors, 2014: The NCEP climate forecast system version 2. *J. Climate*, **27**, 2185–2208, doi:10.1175/JCLI-D-12-00823.1.
- Sandeep, S., and R. S. Ajayamohan, 2014: Origin of cold bias over the Arabian Sea in climate models. *Sci. Rep.*, **4**, 6403, doi:10.1038/srep06403.
- Sayantani, O., and C. Gnanaseelan, 2015: Tropical Indian Ocean subsurface temperature variability and the forcing mechanisms. *Climate Dyn.*, **44**, 2447–2462, doi:10.1007/s00382-014-2379-y.
- , —, J. S. Chowdary, A. Parekh, and S. Rahul, 2016: Arabian Sea SST evolution during spring to summer transition period

- and the associated processes in coupled climate models. *Int. J. Climatol.*, **36**, 2541–2554, doi:10.1002/joc.4511.
- Sen Gupta, A., S. McGregor, E. van Sebille, A. Ganachaud, J. N. Brown, and A. Santoso, 2016: Future changes to the Indonesian Throughflow and Pacific circulation: The differing role of wind and deep circulation changes. *Geophys. Res. Lett.*, **43**, 1669–1678, doi:10.1002/2016GL067757.
- Swapna, P., and Coauthors, 2015: The IITM Earth System Model: Transformation of a seasonal prediction model to a long-term climate model. *Bull. Amer. Meteor. Soc.*, **96**, 1351–1367, doi:10.1175/BAMS-D-13-00276.1.
- Valsala, V., and S. Maksyutov, 2010: A short surface pathway of the subsurface Indonesian Throughflow water from the Java coast associated with upwelling, Ekman transport, and subduction. *Int. J. Oceanogr.*, **2010**, 540783, doi:10.1155/2010/540783.
- Wajsowicz, R. C., 2007: Seasonal-to-interannual forecasting of tropical Indian Ocean sea surface temperature anomalies: Potential predictability and barriers. *J. Climate*, **20**, 3320–3343, doi:10.1175/JCLI4162.1.
- Wang, C., L. Zhang, S. K. Lee, L. Wu, and C. R. Mechoso, 2014: A global perspective on CMIP5 climate model biases. *Nat. Climate Change*, **4**, 201–205, doi:10.1038/nclimate2118.
- Wang, H., A. Kumar, and W. Wang, 2013: Characteristics of subsurface ocean response to ENSO assessed from simulations with the NCEP Climate Forecast System. *J. Climate*, **26**, 8065–8083, doi:10.1175/JCLI-D-12-00795.1.
- Xiang, B., B. Wang, Q. Ding, F.-F. Jin, X. Fu, and H. J. Kim, 2012: Reduction of the thermocline feedback associated with mean SST bias in ENSO simulation. *Climate Dyn.*, **39**, 1413–1430, doi:10.1007/s00382-011-1164-4.
- Xie, S.-P., H. Annamalai, F. A. Schott, and J. P. McCreary, 2002: Structure and mechanisms of South Indian Ocean climate variability. *J. Climate*, **15**, 864–878, doi:10.1175/1520-0442(2002)015<0864:SAMOSI>2.0.CO;2.
- Zhou, L., R. Murtugudde, and M. Jochum, 2008: Seasonal influence of Indonesian Throughflow in the southwestern Indian Ocean. *J. Phys. Oceanogr.*, **38**, 1529–1541, doi:10.1175/2007JPO3851.1.
- Zweng, M. M., and Coauthors, 2013: *Salinity*. Vol. 2, *World Ocean Atlas 2013*, NOAA Atlas NESDIS 74, 39 pp.